lecular weight on a double-logarithmic scale. In both cases excluded volume affects the chain dimensions. The radius of gyration is related to the molecular weight by the expression

$$R_g = 0.17 M_z^{0.58}$$

where M_z is the z average of the molecular weight measured by GPC.

In the semidilute regime, where screening leads to dimensions smaller than in dilute solutions, the experimental values of R_g of the PDMS chains at a concentration $c = c_e$ are significantly different from the radii of gyration of the elastic chains in the corresponding swollen networks.

We can conclude that the conformation of an elastic chain in a swollen network is mainly governed by the local polymer–solvent interaction, whereas the equilibrium swelling degree of the gel depends on the functionality of the junctions points and on the volume fraction v_c at which the network was prepared.

This study corroborates several other investigations on swollen networks[19,22] and strongly supports de Gennes' approach of the behavior of a network swollen at equilibrium in a good solvent.

Acknowledgment. We thank Professor H. Benoit and Dr. P. Rempp for many fruitful and stimulating discussions.

Registry No. Neutron, 12586-31-1.

References and Notes

(1) Beltzung, M.; Picot, C.; Rempp, P.; Herz, J. *Macromolecules* **1982**, *15*, 1594.
(2) Guth, E.; Mark, H. *Monatsh. Chem.* **1934**, *65*, 93.
(3) Wall, F. T. *J. Chem. Phys.* **1943**, *11*, 527.
(4) Flory, P. J. "Principles of Polymer Chemistry"; Cornell University Press: Ithaca, NY, 1953.
(5) James, H. M. *J. Chem. Phys.* **1947**, *15*, 651.
(6) James, H. M.; Guth, E. *J. Chem. Phys.* **1947**, 669. *J. Polym. Sci.* **1949**, *4*, 153.
(7) Flory, P. J. *J. Chem. Phys.* **1977**, *66*, 5720.
(8) Flory, P. J. *Polymer* **1979**, *20*, 1317.
(9) de Gennes, P.-G. "Scaling Concepts in Polymer Physics"; Cornell University Press: Ithaca, NY, 1979.
(10) Akcasu, A. Z.; Summerfield, G. C.; Jahshan, S. N.; Han, C. C.; Kim, C. Y.; Yu, H. *J. Polym. Sci., Polym. Phys. Ed.* **1980**, *18*, 863.
(11) Benoit, H.; Koberstein, J.; Leibler, L. *Makromol. Chem., Suppl.* **1981**, *4*, 85.
(12) Tangari, C.; Summerfield, G. C.; King, J. S.; Berliner, R.; *Macromolecules* **1980**, *13*, 1546.
(13) Wignall, G. D.; Hendricks, R. N.; Koehler, W. C.; Lin, J. S.; Wai, M. P.; Thomas, E. L.; Stein, R. S. *Polymer* **1981**, *22*, 886.
(14) Boue, F.; Nierlich, N.; Leibler, L. *Polymer* **1982**, *23*, 29.
(15) Zimm, B. H. *J. Chem. Phys.* **1948**, *16*, 1093.
(16) Weiss, P.; Herz, J.; Rempp, P *Makromol. Chem.* **1970**, *135*, 249.
(17) Huglin, M. B. "Light Scattering from Polymer Solutions"; Academic Press: London and New York, 1972.
(18) Belkebir-Mrani, A.; Beinert, G.; Herz, J.; Rempp, P. *Eur. Polym. J.* **1977**, *13*, 277.
(19) Candau, S.; Peters, A.; Herz, J. *Polymer* **1981**, *22*, 1504.
(20) Levy, S. Thesis, Strasbourg, 1964. Duplessix, R. Thesis, Strasbourg, 1975.
(21) Pearson, D. S. *Macromolecules* **1977**, *10*, 696.
(22) Bastide, J.; Picot, C.; Candau, S. *J. Macromol. Sci., Phys.* **1981**, B19 (1), 13.

Dynamic Light Scattering Studies of Polymer Solutions. 1. Histogram Analysis of Internal Motions

Yoshisuke Tsunashima, Norio Nemoto, and Michio Kurata*

Institute for Chemical Research, Kyoto University, Uji, Kyoto-fu 611, Japan.
Received July 2, 1982

ABSTRACT: The efficiency of the histogram method in the study of internal motions by dynamic light scattering has been tested for a narrow-distribution polystyrene having a weight-average molecular weight of 5.50×10^6 in dilute solutions in *trans*-decalin at 25 °C. The bimodal histogram analysis has been proved to be adequate for estimating the characteristic parameters of internal relaxation motions separately from those of translational diffusive motions. The results are compatible with theoretical predictions by the non-free-draining chain model with preaveraged hydrodynamic interaction.

Introduction

Dynamic light scattering can be used to study the internal motions of a flexible polymer in dilute solution. For example, the longest intramolecular relaxation time τ_1 is obtainable from the intensity autocorrelation function $A(\tau)$ measured in the intermediate q region, where the reciprocal magnitude q^{-1} of the scattering vector is comparable to the root-mean-square radius of gyration R_G of the polymer. This feature of dynamic light scattering is remarkable, because the τ_1 in dilute solutions can hardly be determined by other means such as viscoelastic measurements.

Several groups of investigators have attempted the two-exponential-term analysis[1-5] or the cumulant analysis[6-9] of $A(\tau)$ to estimate τ_1 or the first cumulant Ω, respectively, and have compared the results with predictions of various theories. However, extrapolation of the estimated values of τ_1 and Ω to zero scattering angle and zero concentration, which is necessary to precisely test the theories, has not been fully performed in these studies. Thus the results are still not conclusive, though two latest studies[5,9] seem to support predictions obtained for the nondraining polymer model with the preaveraged hydrodynamic interaction,[10,11] rather than that without preaveraging.[12]

Chu and co-workers[13] have recently presented the histogram method for determining the distribution of decay rate $G(\Gamma)$ from the measured correlation function $A(\tau)$. The method has been proved to be effective, especially in the analysis of bimodal distributions of Γ which appear, for example, in binary mixtures of polystyrene latex particles of different sizes.[14]

In this paper, we apply the histogram method to the analysis of $A(\tau)$ measured in the intermediate q region and examine whether the method is effective in estimating τ_1 of flexible polymers separately from the translational diffusion coefficient D. For the purpose, we used a nar-

0024-9297/83/2216-0584$01.50/0

row-distribution polystyrene with weight-average molecular weight 5.50×10^6 as a test sample. Measurements of $A(\tau)$ were performed in the range of polymer concentration from 0.5 to 1.3 mg cm^{-3} in *trans*-decalin at scattering angles from 10° to 150° using a computer-controlled software correlator with 512 channels.[15] Extrapolation of the data to zero concentration and zero scattering angle has been performed with great care.

Histogram Analysis of Internal Motions

The normalized intensity autocorrelation function $A(\tau)$ measured by the homodyne method is related to the normalized scattered-field autocorrelation function $g^{(1)}(\tau)$ as

$$A(\tau) = 1 + \beta|g^{(1)}(\tau)|^2 \tag{1}$$

where β is a parameter determined by the experimental condition of coherence. When the distribution of decay rate Γ arises from polydispersity of samples or from multiplicity of molecular motions, the correlation function $g^{(1)}(\tau)$ can be expressed as

$$|g^{(1)}(\tau)| = \int_0^\infty G(\Gamma) \exp(-\Gamma\tau)\, d\Gamma \tag{2}$$

In the histogram method,[13] we approximate the decay-rate distribution $G(\Gamma)$ by an equally segmented histogram extending over a region in Γ space. We denote the lower and upper limits of the region by Γ_{min} and Γ_{max}, the number of histogram steps by m, the width of each step by $\Delta\Gamma$, and the height of the jth step by H_j, respectively. We then have

$$|g^{(1)}(\tau)| = \sum_{j=1}^{m} H_j \int_{\Gamma_j-(\Delta\Gamma/2)}^{\Gamma_j+(\Delta\Gamma/2)} \exp(-\Gamma\tau)\, d\Gamma \tag{3}$$

with the normalization condition

$$\sum_{j=1}^{m} H_j \Delta\Gamma = 1 \tag{4}$$

Obviously, $\Delta\Gamma = (\Gamma_{max} - \Gamma_{min})/m$ and $\Gamma_j = \Gamma_{min} + (j - {}^1/_2)\Delta\Gamma$. Substitution of eq 3 into eq 1 yields

$$A^*(\tau) = 1 + \beta\left(\sum_{j=1}^{m}(-H_j/\tau)\{\exp[-(\Gamma_j + {}^1/_2\Delta\Gamma)\tau] - \exp[-(\Gamma_j - {}^1/_2\Delta\Gamma)\tau]\}\right)^2 \tag{5}$$

where the asterisk represents the computed function. According to the method of least squares, we then minimize the fitting error of the computed function $A^*(\tau)$ to the observed one $A(\tau)$ with respect to each H_j simultaneously:

$$\frac{\partial}{\partial H_j}\sum_i\{[A(i\Delta\tau) - A^*(i\Delta\tau)]^2/\sigma_i^2\} = 0 \qquad (j = 1, 2, ..., m) \tag{6}$$

Here $\Delta\tau$ is the clock pulse interval, i ($=\tau/\Delta\tau$) is the channel number, and the σ_i are the uncertainties in the data points $A(i\Delta\tau)$. The algorithm of Marquardt[16] is used in the curve-fitting computation.

Initial values for H_j and for Γ_{min}, Γ_{max}, and m are to be refined after each computation until $A^*(\tau)$ agrees with $A(\tau)$ to within statistical counting error limits. The refinement of the initial H_j are immaterial, but that of the range and fineness parameters, Γ_{min}, Γ_{max}, and m, requires some care. A typical course of the curve-fitting process is illustrated in Figure 1, where (a) represents an input histogram and (b) represents the output of the computation by eq 6. The $A(i\Delta\tau)$ data used consist of 511 points as shown in Figure 2, which were obtained for a narrow-distribution polystyrene in the intermediate q region. In this computation, we set $H_j = 0$ if the height of a step, say j, comes out smaller than ${}^1/_{200}$ of the highest height in the histogram. It is notable that the output histogram b has already shown the bimodal shape at this stage of the curve-fitting process.

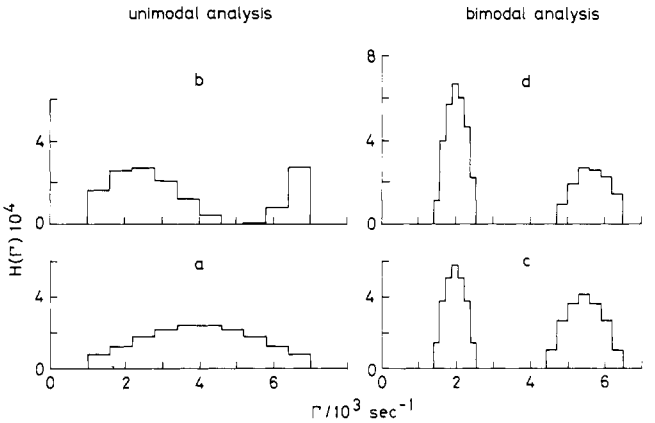

Figure 1. Examples of input and output histograms in the curve-fitting process following eq 6. Histograms a and b are obtained in the unimodal analysis of the autocorrelation function $A(\tau)$ shown in Figure 2, and histograms c and d are obtained in the bimodal analysis of the same $A(\tau)$.

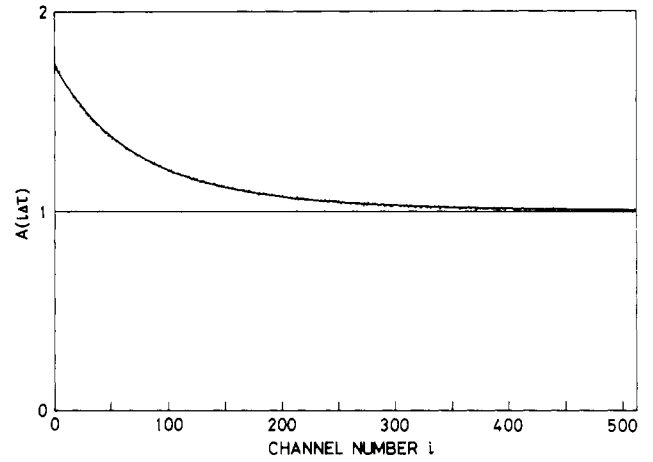

Figure 2. Autocorrelation function $A(i\Delta\tau)$ plotted against channel number i for polystyrene (PS) in *trans*-decalin (tD) at T = 25 °C, θ = 120°, and λ_0 = 488 nm. Data points are denoted by dots and the computed values are represented by the solid curve. Other technical data: $M_w = 5.50 \times 10^6$, $c = 9.15 \times 10^{-4}$ g/cm^3, $\Delta\tau$ = 2 μs, total accumulation number = 1200, and $\Gamma_e\tau_{max} = 3.5$.

We then carry out the search for the optimum-fit histogram by employing bimodal histograms as input for the curve-fitting computation. Denoting by m_l and $\Delta\Gamma_l$ the number of steps and the width of each step in mode l (=1, 2), respectively, we rewrite eq 5 as

$$A^*(\tau) = 1 + \beta\left(\sum_{l=1}^{2}\sum_{j=1}^{m_l}(-H_{lj}/\tau)\{\exp[-(\Gamma_{lj} + {}^1/_2\Delta\Gamma_l)\tau] - \exp[-(\Gamma_{lj} - {}^1/_2\Delta\Gamma_l)\tau]\}\right)^2 \tag{7}$$

with

$$\sum_{l=1}^{2}\sum_{j=1}^{m_l} H_{lj}\Delta\Gamma_l = 1 \tag{8}$$

The fitting procedure for the bimodal histogram is essentially the same as that for the unimodal histogram. Histograms c and d in Figure 1 illustrate an input histogram and an optimum-fit histogram, respectively, which were obtained at the final stage of the curve-fitting process. In this paper, we computed several equally optimum fit

histograms for each set of experimental data $A(i\Delta\tau)$ and used the results for estimating the statistical error of the computed histogram parameters.

In bimodal histograms such as (d), the first slow mode ($l = 1$) may be assigned to the translational diffusive motion of the polymer, and the second mode to the internal motions. We define the fractional amplitude a_l and the mean decay rate $\bar{\Gamma}_l$ for each mode by

$$a_l = \sum_{j=1}^{m_l} H_{lj}\Delta\Gamma_l \qquad (l = 1, 2) \tag{9}$$

$$\bar{\Gamma}_l = a_l^{-1}\sum_{j=1}^{m_l} \Gamma_{lj}H_{lj}\Delta\Gamma_l \qquad (l = 1, 2) \tag{10}$$

respectively. The effective decay rate Γ_e of the whole histogram may then be evaluated as

$$\Gamma_e = \int_0^\infty \Gamma G(\Gamma)\, d\Gamma = a_1\bar{\Gamma}_1 + a_2\bar{\Gamma}_2 \tag{11}$$

The Γ_e is identical with the first cumulant Ω, since we have

$$\Omega = -\lim_{\tau\to 0} d|g^{(1)}(\tau)|/d\tau = \lim_{\tau\to 0}\int_0^\infty \Gamma G(\Gamma)\exp(-\Gamma\tau)\, d\Gamma = \Gamma_e \tag{12}$$

For a monodisperse polymer at infinite dilutions, the correlation function $g^{(1)}(\tau)$ is theoretically expressed as[17]

$$|g^{(1)}(\tau)| = P_0(X)\exp(-q^2D_0\tau) + P_2(X)\exp[-(q^2D_0 + 2\tau_1^{-1})\tau] + \ldots \tag{13}$$

where D_0 is the translational diffusion coefficient and τ_1 is the longest intramolecular relaxation time. The expansion coefficients $P_i(X)$ are called the structure factors and they obey

$$P(X) = P_0(X) + P_2(X) + \ldots = (2/X^2)(e^{-X} - 1 + X) \tag{14}$$

with

$$X = q^2R_G^2 = [(16\pi^2/\lambda^2)\sin^2(\theta/2)]R_G^2 \tag{15}$$

Here θ is the scattering angle, λ the wavelength in medium, and R_G^2 the mean-square radius of gyration.

In the two-exponential-term analysis of $A(\tau)$,[1-5] the truncated form of eq 13 has been used to estimate, by curve fitting, the diffusion coefficient D and the collective intramolecular relaxation time τ_c:

$$|g^{(1)}(\tau)| = b_1\exp(-q^2D\tau) + b_2\exp[-(q^2D + 2\tau_c^{-1})\tau] \tag{16}$$

where b_1 and b_2 are constants.

In the bimodal histogram analysis, the quantities D and τ_c can be newly defined as

$$\bar{\Gamma}_1 = q^2D \tag{17}$$

$$\bar{\Gamma}_2 - \bar{\Gamma}_1 = 2/\tau_c \tag{18}$$

The τ_c thus defined includes contributions from higher relaxation modes than τ_1 and is not the same as that appearing in eq 16 unless the Γ_2 histogram is sufficiently narrow. At infinite dilution, the τ_c given by eq 18 reduces to τ_1 in the limit $X \to 0$. We have also $D = D_0$ and

$$a_1 = P_0(X)/P(X) \tag{19}$$

at infinite dilution.

Experimental Section

We used a narrow-distribution polystyrene (PS) of nominal molecular weight $M_w = 5.53 \times 10^6$ (Toyo Soda Co., sample code FF35, $M_w/M_n = 1.04$) in *trans*-decalin (tD). Dust-free solutions were prepared by centrifugation as described elsewhere.[15] Static light scattering measurements were made with a LS601 photometer (Union Giken) equipped with a He–Ne laser ($\lambda_0 = 633$ nm) at 20.4 °C (Θ temperature), and viscosity measurements were made with Ubbelohde capillary viscometers at 20.4 and 25 °C. The results were $M_w = 5.50 \times 10^6$, $R_{G\Theta}^2 = 4.54 \times 10^{-11}$ cm^2, $[\eta]_\Theta = 183$ cm^3/g, and $[\eta](25\ °C) = 222$ cm^3/g. R_G^2 at 25 °C was estimated as 5.49×10^{-11} cm^2 from these viscosity data. The solvent viscosities η_0 at 20.4 and 25 °C were 2.113×10^{-2} and 1.941×10^{-2} g/(cm s), respectively.

The intensity autocorrelation function $A(\tau)$ was measured at 25 °C for the V_v component of scattered light by using a dynamic light scattering instrument with a time interval digitizer.[15] We used an argon ion laser ($\lambda_0 = 488$ nm) equipped with an etalon as a light source. The scattering angles were set at 10°, 30°, 60°, 90°, 120°, and 150°, which covered the q range such that $0.24 < qR_G < 2.7$ and $0.002 < ql < 0.023$. Here the statistical length of polymer segment l is chosen as 6.3 Å. The condition that $X \ll 1$ was thus realized at $\theta = 10°$ in the present solution. A FACOM M-160 AD computer in our institute was used for data analysis.

Table I
Characteristic Decay Rates for Polystyrene in *trans*-Decalin at $T = 25$ °C

$c/10^{-4}$ g cm^{-3}	$[\bar{\Gamma}_1/\sin^2(\theta/2)]_{\theta\to 0}$/s^{-1}	$(\bar{\Gamma}_2 - \bar{\Gamma}_1)_{\theta\to 0}$/s^{-1}
12.70	2700 ± 30	2180 ± 80
9.15	2700 ± 30	2190 ± 50
7.57	2670 ± 50	2210 ± 60
4.78	2650 ± 40	2230 ± 30
0.0	2650 ± 50	2200 ± 60

Results

A typical example of the intensity autocorrelation function is shown in Figure 2, where $A(i\Delta\tau)$ obtained at $c = 9.15 \times 10^{-4}$ g cm^{-3} and $\theta = 120°$ are plotted against the channel number i. The clock pulse interval $\Delta\tau$ was 2 μs. The optimum-fit histogram was bimodal as shown in Figure 1d. The computed correlation function $A^*(\tau)$ corresponding to this histogram is shown by the solid curve in Figure 2. The histogram parameters obtained by eq 9–11 are $a_1 = 0.585$, $\bar{\Gamma}_1 = 2000$ s^{-1}, $\bar{\Gamma}_2 = 5640$ s^{-1}, and $\Gamma_e = \Omega = 3510$ s^{-1}. These values of $\bar{\Gamma}_1$ and $\bar{\Gamma}_2$ are then substituted in eq 17 and 18 to give $D = 1.86 \times 10^{-8}$ cm s^{-1} and $\tau_c = 549$ μs.

A similar analysis to the above has been performed for $A(i\Delta\tau)$ measured at other scattering angles θ. The optimum-fit histograms obtained for θ larger than 30° were all bimodal, while that for $\theta = 10°$ was unimodal. The angular dependences of the bimodal histogram parameters are shown by unfilled circles in Figure 3. The ratio $\bar{\Gamma}_1/\sin^2(\theta/2)$ is independent of q^2, as expected from eq 17, indicating that the translational diffusive mode has been successfully separated from the internal modes at all scattering angles tested. The quantity $\bar{\Gamma}_2 - \bar{\Gamma}_1$ depends strongly on q in the range of θ higher than about 90°, reflecting contributions from higher modes of internal motions, and it becomes practically constant at lower angles. The amplitude of the diffusive mode, a_1, displays a sigmoidal decrease with increasing q^2.

The values of $[\bar{\Gamma}_1/\sin^2(\theta/2)]_{\theta\to 0}$ and $(\bar{\Gamma}_2 - \bar{\Gamma}_1)_{\theta\to 0}$ obtained at four concentrations are listed in Table I. The former quantity decreases slightly with decreasing concentration, while the latter remains constant to within a 5% error. Extrapolation to zero concentration yields the values added in the bottom of Table I, which are converted to

$$D_0 = 1.84 \times 10^{-8}\ \text{cm}^2\ \text{s}^{-1}$$

$$\tau_1 = 908\ \mu\text{s} \tag{20}$$

The $\bar{\Gamma}_2 - \bar{\Gamma}_1$ obtained at each given θ are also practically independent of c as illustrated in Figure 4. The values of $(\bar{\Gamma}_2 - \bar{\Gamma}_1)_{c\to 0}$ are given in Table II, which exhibits a strong

Table II
$P_0(X)/P(X)$, $\bar{\Gamma}_2 - \bar{\Gamma}_1$, and $\Gamma_e/\sin^2(\theta/2)$ at Infinite Dilution for Polystyrene in *trans*-Decalin at $T = 25\ ^\circ C$

θ/deg	$q^2/10^{10}$ cm^{-2}	X	$[P_0(X)/P(X)]_{c\to 0}/10^{-2}$	$(\bar{\Gamma}_2 - \bar{\Gamma}_1)_{c\to 0}$/s^{-1}	$[\Gamma_e/\sin^2(\theta/2)]_{c\to 0}$/s^{-1}
30	0.964	0.53	97.6 ± 2.0	2190 ± 50	3050 ± 50
60	3.597	1.97	89.5 ± 1.3	2220 ± 40	3740 ± 60
90	7.194	3.95	69.2 ± 1.6	2410 ± 40	4140 ± 30
120	10.79	5.92	56.4 ± 1.1	3450 ± 80	4660 ± 30
150	13.42	7.37	49.2 ± 1.2	5030 ± 110	5170 ± 70

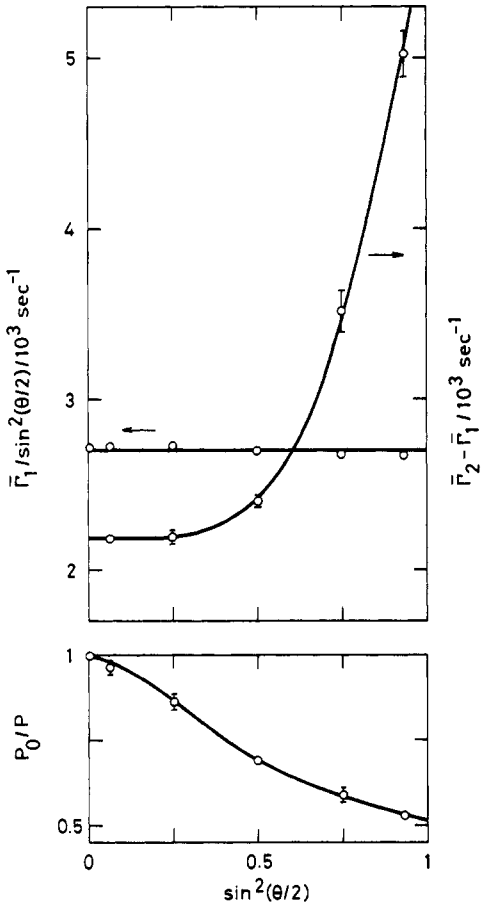

Figure 3. Translational diffusive decay rate $\bar{\Gamma}_1/\sin^2(\theta/2)$, the collective intramolecular relaxation rate $\bar{\Gamma}_2 - \bar{\Gamma}_1$, and the relative scattered intensity of the translational mode $P_0(X)/P(X)$, each plotted against $\sin^2(\theta/2)$. Polymer concentration $c = 9.15 \times 10^{-4}$. The vertical bars attached to data points represent fitting uncertainties in the histogram analysis, which are smaller than 4% for $\bar{\Gamma}_2 - \bar{\Gamma}_1$ over the tested region of scattering angles, 30°–150°.

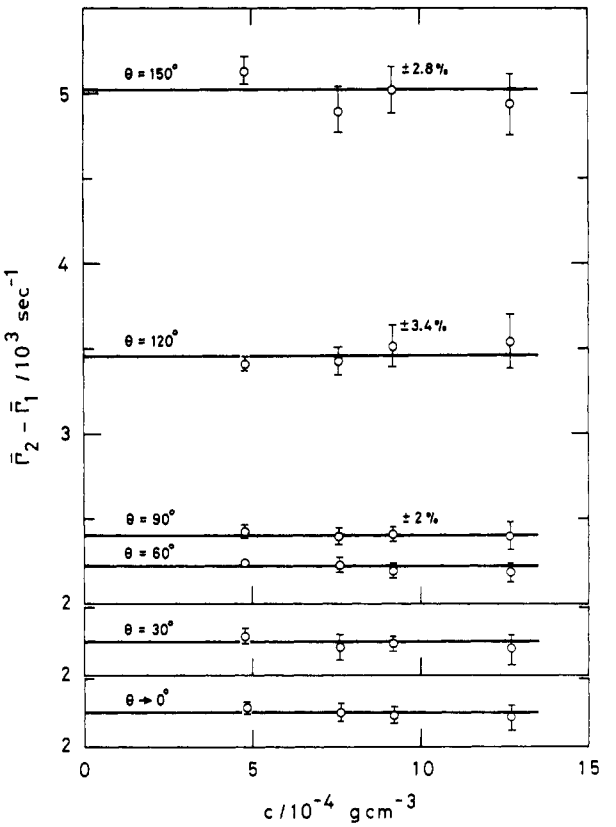

Figure 4. Plots of $\bar{\Gamma}_2 - \bar{\Gamma}_1$ against the polymer concentration c at five scattering angles tested and at zero angle. The vertical bars bear the same meanings as in Figure 3.

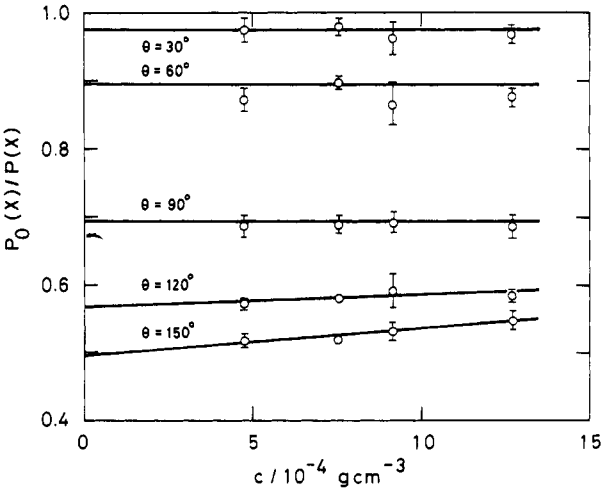

Figure 5. Plots of $P_0(X)/P(X)$ against the polymer concentration c at five scattering angles tested. The vertical bars bear the same meanings as in Figure 3.

dependence on q, actually a q^ν dependence with $\nu > 2.3$, in the range $X > 5$, and becomes constant in the range $X < 2$.

Figure 5 shows the concentration dependence of a_1 at five scattering angles. This quantity is constant at low scattering angles, say 30° or 60°, but shows a weak positive dependence on c at high angles, say 120° and 150°. The linear extrapolation of a_1 to zero concentration allows us to estimate the structure factor $[P_0(X)/P(X)]_{c\to 0}$. The results are shown in Table II.

Discussion

The longest intramolecular relaxation time τ_1 can be expressed in the form

$$\tau_1 = M\eta_0[\eta]/A_1RT \qquad (21)$$

where M is the molar mass of the polymer, R is the gas constant, and T is the absolute temperature. The numerical factor A_1 is 0.822 for the free-draining Rouse chain,[18] 1.184 for the non-free-draining chain with preaveraged hydrodynamic interaction,[10,11] and 0.574 for the non-free-draining chain without preaveraging.[12] Substitution of the present results, i.e., $\tau_1 = 908\ \mu$s, $M = 5.50 \times 10^6$, $[\eta] = 222$ cm^3 g^{-1}, and $\eta_0 = 1.941 \times 10^{-2}$ g cm^{-1} s^{-1}, into eq 20 yields $A_1 = 1.06 \pm 0.03$, which is close to the Zimm value, 1.184.

In Figure 6, the structure factor $[P_0(X)/P(X)]_{c\to 0}$ is

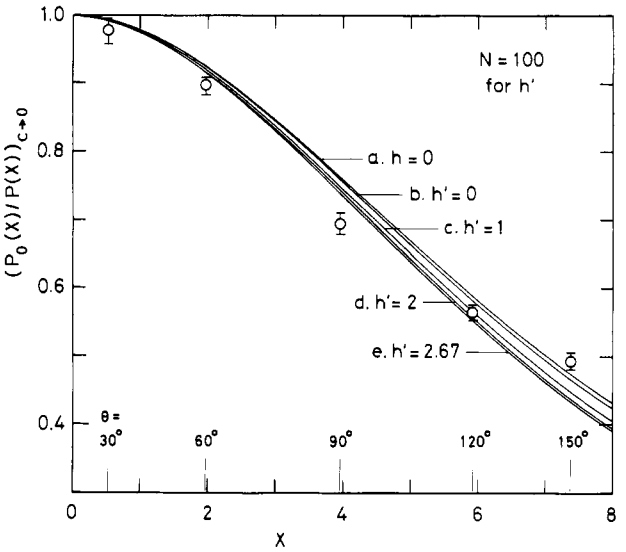

Figure 6. Structure factor $(P_0(X)/P(X))_{c\to 0}$ plotted against X and its theoretical values obtained for a variety of magnitude of hydrodynamic interactions: Curve a, free-draining ($h = 0$, $N \gg 1$);[17] curve b, free-draining ($h' = 0$, $N = 100$);[19] curve c, partial draining ($h' = 1$, $N = 100$);[19] curve d, partial draining ($h' = 2$, $N = 100$);[19] curve e, non-free-draining ($h' = 2.67$, $N = 100$).

shown as a function of X, where unfilled circles represent the present experimental data and solid curves represent various theoretical calculations. Curve a, designated as $h = 0$, represents the analytical calculations for a free-draining chain consisting of a large number of chain segments.[17] Curves b–e represent the numerical results obtained for a chain consisting of 100 segments,[19] with the associated $h' = 0$ denoting the free-draining case, $h' = 2.67$ the non-free-draining case, and $h' = 1$ and 2 two partially draining cases. In these theories, the preaveraged Oseen tensor has been used to describe the hydrodynamic interaction between segments. On the whole, our experimental data seem to support the non-free-draining model.

Using eq 11, we can obtain the effective decay rates at zero concentration, $(\Gamma_e)_{c\to 0}$; these are shown in the last column of Table II and are to be compared with theoretical curves for the first cumulant Ω. All the data points of $(\Gamma_e/\bar{\Gamma}_1)_{c\to 0}$ lie close to the theoretical curve derived for a non-free-draining Zimm model, though the curve is not shown here. Three values of $(\Gamma_e)_{c\to 0}$ obtained at high scattering angles, 90°, 120° and 150°, exhibit the q^ν dependence with $\nu = 2.73$, which is slightly smaller than the asymptotic value, $\nu = 3$, for large values of q.

In conclusion, the histogram method is effective for estimating the internal motions of flexible polymers separately from the translational diffusive motion and the bimodal histogram parameters $\bar{\Gamma}_1$, $\bar{\Gamma}_2 - \bar{\Gamma}_1$, a_1, and Γ_e give important information concerning the polymer chain dynamics. We have also noticed that in the vicinity of Θ temperature the dynamic behavior of polymer chains can be well described by the non-free-draining chain model with preaveraged hydrodynamic interaction.

Appendix

It is obvious that the output of each computation following eq 6 depends heavily on the input histogram. For example, in the case illustrated in Figure 1, an optimum-fit histogram such as (d) is obtainable only when an appropriate bimodal input has been employed. The unimodal analysis also gives a bimodal histogram like (b) if the number of histogram steps m is about 10, but for larger values of m, say 30, it gives an almost meaningless histogram that contains many steps with negative heights, $H_j < 0$. The negative steps, which are essentially noise in the curve-fitting computation, become notable first in the empty region, where no substantial distribution of Γ exists, and then expand into the substantial region as m increases or the step width $\Delta\Gamma$ decreases. Thus in the histogram analysis, it is essential to choose appropriate values for m or $\Delta\Gamma$ according to the nature of given data $A(i\Delta\tau)$ as well as the number of data points and the uncertainty involved in each point.

The appropriate number of steps m can be most conveniently estimated by analyzing the simulated data of $A(i\Delta\tau)$ for some typical distributions $G(\Gamma)$ as described in the preceding paper.[14] We constructed there the simulated data $A(i\Delta\tau)$ by introducing a plausible counting error into the theoretical values $A^\circ(i\Delta\tau)$ calculated by eq 1 and 2 or, more precisely, by adding to the $A^\circ(i\Delta\tau)$ at each of 512 data points a random number generated in the range bounded by $\pm[0.03A^\circ(\Delta\tau)]$. Using the data $A(i\Delta\tau)$ thus simulated, we have found that the appropriate value of m is 14–20 if the total time range extends to $512\Delta\tau \simeq 2/\Gamma_e$ and that the original bimodal distributions $G(\Gamma)$ can be recovered by the optimum-fit histograms with the following reliances: (1) 99% on Γ_e, 95% on μ_2, and 90% on μ_3 and μ_4 for the whole distribution and (2) 99% on $\bar{\Gamma}_l$, 75% on μ_{2l}, the correct order of magnitude on μ_{3l} and μ_{4l}, and 95% on a_l for constituent distributions l (=1 and 2).[14] Here Γ_e is the effective decay rate defined by eq 11, μ_n is the nth moment about Γ_e defined by

$$\mu_n = \int_0^\infty (\Gamma - \Gamma_e)^n G(\Gamma)\, d\Gamma \qquad \text{(A.1)}$$

and a_l is the fractional amplitude of mode l. In addition, it has been confirmed that the third- and fourth-order cumulant analyses also give Γ_e and μ_2 with the same order of reliability as above if the total time range analyzed is kept unchanged.

Based on the above results, we carried out the histogram analysis in the following way.

(1) The cumulant analysis has been performed to obtain approximate values of Γ_e and μ_2/Γ_e^2 in advance of the histogram analysis. These parameters are useful for setting the total time range appropriately and also for determining the unimodal input histogram with which the analysis is initiated.

(2) If the unimodal analysis gives a bimodal output, we immediately switch to the bimodal analysis.

(3) Steps with negative heights also appear in the bimodal analysis if the input histogram ranges, $\Gamma_{l\min}$ and $\Gamma_{l\max}$ ($l = 1$ or 2), appreciably overlap the empty region. This behavior can be effectively utilized for improving input histograms.

(4) The relative fitting error, $|A^*(i\Delta\tau) - A(i\Delta\tau)|/A(i\Delta\tau)$, for final optimum-fit histograms should be less than 0.3%, about one-tenth of the plausible maximum counting error, at most data points. Of course, no systematic deviation is allowed.

We were able to obtain, according to the above procedure and criteria, final results that do not depend on the initial input histogram. Finally, we note that only the translational mode becomes observable at the lowest scattering angle 10°. Very precise results are obtained by the unimodal analysis in this case, and the results are consistent with the results of bimodal analysis at higher angles as described in the text.

Registry No. Polystyrene, 9003-53-6.

References and Notes

(1) Huang, W.-N.; Frederick, J. E. *J. Chem. Phys.* **1973**, *58*, 4022. *Macromolecules* **1974**, *7*, 34.

(2) King, T. A.; Knox, A.; McAdam, J. D. G. *Chem. Phys. Lett.* **1973**, *19*, 351.
(3) McAdam, J. D. G.; King, T. A. *Chem. Phys. Lett.* **1974**, *28*, 90.
(4) King, T. A.; Treadaway, M. F. *J. Chem. Soc., Faraday Trans. 2* **1976**, *72*, 1473.
(5) Jones, G.; Caroline, D. *Chem. Phys.* **1979**, *37*, 187.
(6) Buldt, G. *Macromolecules* **1976**, *9*, 606.
(7) Hendrix, J.; Saleh, B.; Gnadig, K.; DeMaeyer, L. *Polymer* **1977**, *18*, 10.
(8) Freire, J. J. *Polymer* **1978**, *19*, 1441.
(9) Han, C. C.; Akcasu, A. Z. *Macromolecules* **1981**, *14*, 1080.
(10) Zimm, B. H. *J. Chem. Phys.* **1956**, *24*, 269.
(11) Benmouna, M.; Akcasu, A. Z. *Macromolecules* **1978**, *11*, 1187.
(12) Bixon, M.; Zwanzig, R. *J. Chem. Phys.* **1978**, *68*, 1890.
(13) Gulari, E.; Gulari, E.; Tsunashima, Y.; Chu, B. *J. Chem. Phys.* **1979**, *70*, 3965. Gulari, E.; Gulari, E.; Tsunashima, Y.; Chu, B. *Polymer* **1979**, *20*, 347.
(14) Tsunashima, Y.; Nemoto, N.; Makita, Y.; Kurata, M. *Bull. Inst. Chem. Res., Kyoto Univ.* **1981**, *59*, 293.
(15) Nemoto, N.; Tsunashima, Y.; Kurata, M. *Polym. J.* **1981**, *13*, 827.
(16) Marquardt, D. W. *J. Soc. Ind. Appl. Math.* **1963**, *11*, 431.
(17) Pecora, R. *J. Chem. Phys.* **1965**, *43*, 1562; **1968**, *49*, 1032.
(18) Rouse, P. E. *J. Chem. Phys.* **1953**, *21*, 1272.
(19) Perico, A.; Piaggio, P.; Cuniberti, C. *J. Chem. Phys.* **1975**, *62*, 2690, 4911.

Ruthenium Tetraoxide Staining of Polymers for Electron Microscopy

John S. Trent,† Jerry I. Scheinbeim,* and Peter R. Couchman

Department of Mechanics and Materials Science, Rutgers, The State University of New Jersey, Piscataway, New Jersey 08854. *Received January 7, 1982*

ABSTRACT: The need for selective staining agents to enhance electron density contrast for transmission electron microscope (TEM) studies of heterogeneous polymer systems is widely acknowledged. In this study, we describe the use of ruthenium tetraoxide as a staining agent for thin films of various polymers for examination in the TEM. Ruthenium tetraoxide is shown to stain both saturated and unsaturated polymer systems that contain in their unit structure ether, alcohol, aromatic, or amide moieties. High-density polyethylene, linear polyethylene wax, poly(vinyl methyl ketone), and both isotactic and atactic polypropylene were also stained. Ruthenium tetraoxide did not stain poly(methyl methacrylate), poly(vinyl chloride), poly(vinylidene fluoride), and polyacrylonitrile. Optical and electron micrographs demonstrating the utility of this staining agent are presented and the action of RuO_4 on the stained polymers is discussed in terms of previously reported RuO_4–small molecule interactions.

1. Introduction

1.1. General. It is well-known that the micromorphology of polymeric materials is dependent on their heat treatment, composition, and processing and that in turn mechanical properties of these materials such as toughness, impact strength, resilience, fatigue, and fracture strength can be highly sensitive to morphology. Consequently, an explanation of these (and other) mechanical properties should include the nature of relations between heat treatment, composition, and consequent physical microstructure. The transmission electron microscope (TEM) is an established instrument for the characterization of the structure of heterogeneous polymer systems at a high level of resolution. However, it is often necessary to enhance image contrast for polymers by use of a staining agent. Although osmium tetraoxide is useful for unsaturated polymers, a suitable image-contrast enhancing stain for saturated polymers has been lacking. This situation has been improved somewhat by independent reports[1,2] of the discovery of ruthenium tetraoxide (RuO_4) as an effective staining agent for the TEM examination of morphology in both saturated and unsaturated polymeric systems. Vitali and Montani[1] observed improved image contrast for polybutadiene lattices, a terpolymer of acrylonitrile, butadiene, and styrene (ABS), and an acrylonitrile–styrene–acrylonitrile (ASA) polymer. Trent, Scheinbeim, and Couchman[2] demonstrated the usefulness of RuO_4 vapor staining in TEM studies of polystyrene/poly(methyl methacrylate) (PS/PMMA) blends and high-impact polystyrene (HIPS) films, due in both cases to a preferential action of the stain on the PS component.

The purpose of the present study is to determine which types of polymers are stained effectively by RuO_4 for examination in the TEM. Polymer films containing aromatic, ether, alcohol, amide, olefin, ester, nitrile, sulfone, halogen, carbonyl, or unsaturated moieties were exposed to RuO_4 vapor for various times; optical and electron micrographs of the results are presented and the interaction of the staining agent with each polymer is discussed.

1.2. Ruthenium Tetraoxide. Ruthenium, discovered in 1826,[3] is a rare metal[4] in the platinum group and is known to exist in ten different oxidation states (−2, 0, 1, 2, 3, 4, 5, 6, 7, 8),[5,6] of which ruthenium tetraoxide occurs in the 8th state. Although ruthenium tetraoxide was first prepared in 1860,[7] it was not used as an oxidant for organic compounds until 1953.[8] Typically, it is prepared by the oxidation of ruthenium compounds of lower oxidation states (usually ruthenium trichloride, ruthenate ion, or hydrated ruthenium dioxide).[9] Hydrated ruthenium dioxide ($RuO_2 \cdot 2H_2O$)[10,11] has been suggested as the most convenient starting material for the preparation of RuO_4 by a reaction with an excess of sodium periodate ($NaIO_4$) in water, followed by extraction of the tetraoxide with carbon tetrachloride.

Ruthenium tetraoxide is a far more vigorous oxidant than OsO_4;[3,10] many organic compounds that are inert to oxidation by OsO_4 react readily with RuO_4.[8-10,12,13] This highly reactive oxidant was first used as a fixative and stain for electron microscopy by Gaylarde and Sarkany.[14] When

† Present address: Department of Materials Science and Engineering, Polymers Program, The Pennsylvania State University, University Park, Pennsylvania 16802.

0024-9297/83/2216-0589$01.50/0